MIT Libraries | DSpace@MIT

MIT Open Access Articles

Modeling of GaN/AlN heterostructure-based nano pressure sensors

The MIT Faculty has made this article openly available. ***Please share*** how this access benefits you. Your story matters.

Citation: Patil, S., N. Sinha, and R. V. N. Melnik. "Modeling of GaN/AlN heterostructure-based nano pressure sensors." Nanoengineering: Fabrication, Properties, Optics, and Devices VI. Ed. Elizabeth A. Dobisz & Louay A. Eldada. San Diego, CA, USA: SPIE, 2009. 74020C-8. © 2009 SPIE--The International Society for Optical Engineering

As Published: http://dx.doi.org/10.1117/12.826267

Publisher: The International Society for Optical Engineering

Persistent URL: http://hdl.handle.net/1721.1/52740

Version: Final published version: final published article, as it appeared in a journal, conference proceedings, or other formally published context

Terms of Use: Article is made available in accordance with the publisher's policy and may be subject to US copyright law. Please refer to the publisher's site for terms of use.

Massachusetts Institute of Technology

Modeling of GaN/AlN Heterostructure-Based Nano Pressure Sensors

S. Patil[a], N. Sinha[b] and R.V.N. Melnik[a]

[a]M^{2}NeT Lab, Wilfrid Laurier University, Waterloo, ON N2L 3C5, Canada
[b]Department of Mechanical Engineering, Massachusetts Institute of Technology, Cambridge, MA 02139, USA

ABSTRACT

We quantify the influence of thermopiezoelectric effects in nano-sized $Al_xGa_{1-x}N/GaN$ heterostructures for pressure sensor applications based on the barrier height modulation principle. We use a fully coupled thermoelectromechanical formulation, consisting of balance equations for heat transfer, electrostatics and mechanical field. To estimate the vertical transport current in the heterostructures, we have developed a multi-physics model incorporating thermionic emission, thermionic field emission, and tunneling as the current transport mechanisms. A wide range of thermal (0-300 K) and pressure (0-10 GPa) loadings has been considered. The results for the thermopiezoelectric modulation of the barrier height in these heterostructures have been obtained and optimized. The calculated current shows a linear decrease with increasing pressure. The linearity in pressure response suggests that $Al_xGa_{1-x}N/GaN$ heterostructure-based devices are promising candidates for pressure sensor applications under severe environmental conditions.

Keywords: Pressure sensor, $Al_xGa_{1-x}N/GaN$ heterostructures, thermoelectromechanical effects, coupled multiphysics models

1. INTRODUCTION

There has been a recent increase in demand for ultrasensitive, fast, portable and robust pressure sensors that can operate in harsh environments. Materials such as GaN and AlN exhibit favorable thermal, mechanical, and chemical stabilities and radiation hardness with minimal problems arising from the unwanted optical or thermal generation of charge carriers as a result of their large band gap and atomic bondings.[1] Therefore they are suitable materials for constructing pressure sensors for applications in extreme environments. One of the unique advantages of GaN-based devices is that GaN/AlN heterostructures develop sheet charges at the hetero-interfaces due to spontaneous polarizations and piezoelectric polarization.[2–6] The stress-induced modulation of the barrier height in AlGaN/GaN structures has been recently investigated, demonstrating potential use of these structures in pressure or stress sensing.[7–10] Also, portability of a sensor device, one of the prior concerns in sensor applications, can be achieved with recent progress in nano-fabrication techniques. Recent reports on micro pressure sensors based on $Al_xGa_{1-x}N/GaN$ heterostructures grown on 6H:SiC substrate[7] show that the proposed heterostructure is a promising candidate. However, the device peroformace was limited due to the substrate material (6H:SiC), which can be improved further by using substrate from the same family of materials such as GaN.[7] In order to meet technological requirements of such sensors, a systematic study of thermoelectromechanical loading effects in nano-sized heterostrctures is required.

In this work, the pressure response of an $Al_xGa_{1-x}N/GaN$ is investigated using a generalized fully coupled thermoelectromechanical model. We use a fully coupled thermopiezoelectric formulation, consisting of balance equations for heat transfer, electrostatics and mechanical field. Accordingly, the changes in current due to thermionic emission, thermionic field emission and tunneling have been calculated. The results for the thermopiezoelectric modulation of the barrier height in these heterostructures have been obtained. The energy band

Further author information: (Send correspondence to R.V.N. Melnik)
S. Patil: E-mail: spatil@wlu.ca, Telephone: 1 519 884 0710 ext. 2801
N. Sinha: E-mail: nsinha@mit.edu, Telephone: 1 617 715 5238
R.V.N. Melnik: E-mail: rmelnik@wlu.ca, Telephone: 1 519 884 0710 ext. 3662

Nanoengineering: Fabrication, Properties, Optics, and Devices VI, edited by Elizabeth A. Dobisz, Louay A. Eldada,
Proc. of SPIE Vol. 7402, 74020C · © 2009 SPIE · CCC code: 0277-786X/09/$18 · doi: 10.1117/12.826267

Downloaded from SPIE Digital Library on 17 Mar 2010 to 18.51.1.125. Terms of Use: http://spiedl.org/terms

gap shifts for the wide range of thermoelectromechanical loadings have been analyzed. We also study the effect of composition and dimensions of heterostructures on device performance. In particular, we have investigated the devices fabricated on a GaN substrate with the objective of determining the most promising AlGaN/GaN heterostructures for pressure sensing.

2. MODEL FORMULATION

In what follows, we formulate a mathematical model in order to study thermoelectromechanical effects in QDs. A general three-dimensional (3D) axisymmetric model is developed with coupled multi-physics governing equations. The problem is governed by a coupled system of equilibrium equations of elasticity, electrostatics and heat transfer.

2.1 Explicit form of governing equations for wurtzite nanostructures in cylindrical coordinates

Governing equations for wurtzite structures are axisymmetric, hence all thermal-, electric- and mechanical- field solutions are axisymmetric as well. Therefore, the original 3D problem can be reduced in this case to a simpler 2D problem.[4] The electromechanical balance equations in the cylindrical coordinates for axisymmetric case take the following form:[11]

$$\frac{\partial \sigma_{rr}}{\partial r} + \frac{\partial \sigma_{rz}}{\partial z} + \frac{\sigma_{rr} - \sigma_{\theta\theta}}{r} = 0, \tag{1}$$

$$\frac{\partial \sigma_{rz}}{\partial r} + \frac{\partial \sigma_{zz}}{\partial z} + \frac{1}{r}\sigma_{rz} = 0, \tag{2}$$

$$\frac{\partial D_r}{\partial r} + \frac{\partial D_z}{\partial z} + \frac{1}{r} D_r = 0. \tag{3}$$

Here σ_{ij} are stress tensor components, D_i are electric displacement vector components, h_i are the components of heat flux vector. Coupling of equations (1-3) is implemented through constitutive equations. These equations are invariant with respect to rotations around the z axis (in spite of the lack of axisymmetry of the underlying wurtzite lattice, refer to detailed discussions in[12]), hence solutions can be separated into a (r, z) part and a ϕ part, subject to adequate boundary conditions. The constitutive relations in equations then take the following form for wurtzite nanostructures:

$$\begin{aligned}
\sigma_{rr} &= C_{11}\varepsilon_{rr} + C_{12}\varepsilon_{\theta\theta} + C_{13}\varepsilon_{zz} - e_{31}E_z - \beta_{11}\Theta, \\
\sigma_{rz} &= C_{44}\varepsilon_{rz} - e_{15}E_r, \\
\sigma_{zz} &= C_{13}\varepsilon_{rr} + C_{13}\varepsilon_{\theta\theta} + C_{33}\varepsilon_{zz} - e_{33}E_z - \beta_{33}\Theta, \\
D_r &= e_{15}\varepsilon_{rz} + \in_{11} E_r, \\
D_z &= e_{31}\varepsilon_{rr} + e_{31}\varepsilon_{\theta\theta} + e_{33}\varepsilon_{zz} + \in_{33} E_z + p_3\Theta + P^{sp},
\end{aligned} \tag{4}$$

where $c_{ij}, e_{ij}, \in_{ij}$ and κ_{ij} are the elastic moduli, piezoelectric constants, dielectric constants and coefficients of heat conduction, respectively, while p_i and β_{ij} are pyroelectric and stress-temperature material constants, respectively. P^{sp} is the spontaneous polarization. At thermal equilibrium, the temperature change becomes spatially independent, effectively leading to the determination of solution of the equilibrium equations for mechanical and electric field only.[13] The well-posedness of the corresponding mathematical models in this and in more general case was shown in[11,14] (see also references therin) while the analysis of the special types of boundary conditions was carried out in.[15]

To take into account the lattice mismatch, the strain tensor components take the following form:

$$\begin{aligned}
\varepsilon_{rr} &= \frac{\partial u_r}{\partial r} - \varepsilon_a^* \\
\varepsilon_{zz} &= \frac{\partial u_z}{\partial z} - \varepsilon_c^* \\
\varepsilon_{\theta\theta} &= \frac{u_r}{r} - \varepsilon_a^*
\end{aligned}$$

Downloaded from SPIE Digital Library on 17 Mar 2010 to 18.51.1.125. Terms of Use: http://spiedl.org/terms

$$\varepsilon_{rz} = \frac{1}{2}\left(\frac{\partial u_r}{\partial z} + \frac{\partial u_z}{\partial r}\right), \tag{5}$$

with $\varepsilon_a^* = \frac{a_m - a_{QD}}{a_m}$ and $\varepsilon_c^* = \frac{c_m - c_{QD}}{c_m}$ inside the QD and zero otherwise. Quantities, a_m, c_m and a_{QD}, c_{QD} are the lattice constants of the matrix and the QD, respectively, while quantities, ε_a^* and ε_c^* are the local intrinsic strains (lattice mismatch) along a and c directions, respectively. The directions a and c correspond to the shorter and longer dimensions of the unit cell of the wurtzite crystal, respectively.

2.2 Barrier height calculations

In order to highlight further our point regarding the influence of thermoelectromechanical effect, we consider a two band model that consists of conduction band (C_1) and valance band (HH_1). It is instructive in this context to think of electrons and holes as being particles moving in effective potentials, V_{Ceff} and V_{Heff}, respectively. We express the relations for the effective conduction and valance band edges (for wurtzite crystals):

$$E_{C1} = V_{Cedge} + a_c^{\parallel}\varepsilon_{rr} + a_c^{\perp}\varepsilon_{zz} - V, \tag{6}$$

$$E_{HH} = V_{Hedge} + (d_2 + d_4 - d_5)\varepsilon_{rr} + (d_1 + d_3)\varepsilon_{zz} - V, \tag{7}$$

where V_{Cedge} and V_{Hedge} are the unstrained conduction and valance band-edges, respectively, $a_c^{\perp}$ and $a_c^{\parallel}$ are the conduction band deformation potentials along a and c directions, while d_i (i=1,2..5) are valance band deformation potentials.[16]

Hence, the effective band gap ($C_1 - HH_1$) is,

$$\begin{aligned} E_{geff} &= E_{C1} - E_{HH} \\ &= E_g(\Theta) + \left(a_c^{\parallel} - (d_2 + d_4 - d_5)\right)\varepsilon_{rr} + \left(a_c^{\perp} - (d_1 + d_3)\right)\varepsilon_{zz}, \end{aligned} \tag{8}$$

where

$$E_g(\Theta) = E_g(0) - \frac{\alpha_\Theta \Theta^2}{\beta_\Theta + \Theta}, \tag{9}$$

along with α_θ and β_θ as Varshni coefficients.[18]

In this relatively simple case the above equation indicates that the effective energy band gap is independent of electric potential and is dependent on temperature and strain. The electric potential (V) tilts the energy bands, however, the effective band gap remains unchanged.[2]

2.3 Current calculation

As mentioned previously, we calculate transport current under pressure by incorporating thermionic emission and tuneling as the current transport mechanisms. The detailed expressions for the current densities in corresponding cases are expressed as follows. The charge density ρ near the junction is given by[19]

$$\rho(x) = \begin{cases} -qN_a & -x_p < x < 0 \\ +qN_D & 0 < x < x_N, \end{cases} \tag{10}$$

where N_a is the net acceptor concentration in the p side and N_D is the net donor concentration on the N side. Using Gauss's law, one can write

$$\frac{d}{dx}E(x) = \begin{cases} -\frac{qN_a}{\varepsilon_p} & -x_p < x < 0 \\ +\frac{qN_D}{\varepsilon_N} & 0 < x < x_N, \end{cases} \tag{11}$$

where E is the electric field, and ε_p and ε_N are the permittivity in the p and N regions, respectively. According to Gauss's law, the slope of the $E(x)$ profile is given by the charge density divided by the premittivity, Therefore,

$$E(x) = \begin{cases} -\frac{qN_a(x+x_p)}{\varepsilon_p} & -x_p < x < 0 \\ +\frac{qN_D(x-x_N)}{\varepsilon_N} & 0 < x < x_N, \end{cases} \tag{12}$$

Downloaded from SPIE Digital Library on 17 Mar 2010 to 18.51.1.125. Terms of Use: http://spiedl.org/terms

in the depletion region and zero outside. The relationship between the electric field and the electrostatic potential distribution $\phi(x)$ across the junction is given by

$$E_x = -\frac{d}{dx}\phi(x). \tag{13}$$

If the reference potential is chosen as zero for $x < -x_p$, we have

$$\phi(x) = \begin{cases} 0 & x \le -x_p \\ \frac{qN_a(x+x_p)^2}{2\varepsilon_p} & -x_p \le x \le 0 \\ \frac{qN_a x_p^2}{2\varepsilon_p} + \frac{qN_D(2xx_N - x^2)}{2\varepsilon_N} & 0 \le x \le x_N \\ V_0 & x_N \le x, \end{cases} \tag{14}$$

where

$$V_0 = V_{0p} + V_{0N};$$

$$V_{0p} = \phi(0) = \frac{qN_a x_p^2}{2\varepsilon_p};$$

$$V_{0N} = \frac{qN_D x_N^2}{2\varepsilon_N}, \tag{15}$$

where V_0 is the total potential drop across the junction, V_{0p} is the portion of the voltage drop on the p side and V_{0N} is the portion of the voltage drop on the N side. For nondegenerate semiconductors, one can write

$$E_{CN} - F_N \simeq -k_B T \ln\left(\frac{N}{N_{CN}}\right), \tag{16}$$

$$F_p - E_{vp} \simeq -k_B T \ln\left(\frac{p}{N_{vp}}\right). \tag{17}$$

Using the boundary condition $N_a x_p = N_D x_N$, the expressions for V_0, V_{0p}, V_{0N} and the total width of the depletion region x_w from

$$x_w = x_p + x_N, \tag{18}$$

one can derive

$$x_p = \frac{N_D}{N_a + N_D} x_w; \quad x_N = \frac{N_a}{N_a + N_D} x_w. \tag{19}$$

Therefore, x_w and V_0 are related as

$$x_w = \left[\frac{2\varepsilon_p V_0}{qN_a N_D\left(N_D + \frac{\varepsilon_p}{\varepsilon_N} N_a\right)}\right]^{1/2} (N_a + N_D). \tag{20}$$

The band edge $E_v(x)$ from the p side to the N side is expressed as

$$E_v(x) = \begin{cases} -q\phi(x) & \text{on } p \text{ side} \\ -\Delta E_v(x) - q\phi(x) & \text{on } N \text{ side,} \end{cases} \tag{21}$$

The conduction band edge $E_c(x)$ is above $E_v(x)$ by an amount E_{gp} on the p side and by an amount E_{GN} on the N side. $E_c(x)$ is always parallel to $E_v(x)$:

$$E_c(x) = \begin{cases} E_v(x) + E_{gp} & x < 0 \\ E_v(x) + E_{GN} & x > 0, \end{cases} \tag{22}$$

Downloaded from SPIE Digital Library on 17 Mar 2010 to 18.51.1.125. Terms of Use: http://spiedl.org/terms

Using the one-dimensional WKB approximation, the transmission probability for the barrier is expressed as[20]

$$T(E_x) = \begin{cases} \exp\Big(-\frac{4\pi}{h}\int_0^{X_E} [2m_n^*\{E_c(x) - E_x\}]^{1/2} dx \Big), & E_{min} \le E_x < E_{CN}, \\ 1, & E_{CN} \le E_x, \end{cases} \tag{23}$$

where h is Planck constant, m_n^* is the electron effective mass, E_x is the energy coponent in the x direction and $E_{min} = max[E_{cp}, E_c(W)]$.

Assuming the Boltzmann energy distribution, the electron current density J_n across the heterointerface is expressed as

$$\begin{aligned} J_n &= J_{n_1} - J_{n_2} \\ &= -\frac{A^*T}{k}\int_{E_{min}}^{x} f_1(E_x)T(E_x)dE_x + \frac{A^*T}{k}\int_{E_{min}}^{x} f_2(E_x)T(E_x)dE_x \ , \end{aligned} \tag{24}$$

where k is the Boltzmann constant, A^* is the effective Richardson constant for electrons and $f_{1,2}(E_x)$ is the occupation probability in each region. We have

$$J_{n_1}(0^-) = -qv_{n_1}(1+\delta)n_1(0^-)\exp\left(-\frac{\Delta E_c}{kT} \right) , \tag{25}$$

where

$$n_1(0^-) = N_{c1}\exp\left(\frac{E_{fn_1}(0^-) - E_c(0^-)}{kT} \right) , \tag{26}$$

$$v_{n_1} = \frac{A^*T^2}{qN_{c_1}} \ . \tag{27}$$

$$\begin{aligned} \delta = \frac{\exp\left(\frac{E_c(0^+)}{kT}\right)}{kT} \int_{E_{min}}^{E_c(0^+)} \exp\left(-\frac{E_x}{kT} \right) \\ \times\exp\Big(-\frac{4\pi}{h}\int_0^{X_E} [2m_n^*\{E_c(x) - E_x\}]^{1/2} dx \Big) dE_x \ . \end{aligned} \tag{28}$$

Similarly, the equation for the opposing flux of electron current can be expressed as

$$J_{n_2}(0^+) = -qv_{n_2}(1+\delta)n_2(0^+) \ , \tag{29}$$

where

$$n_2(0^+) = N_{c_2}\exp\left(\frac{E_{fn_2}(0^+) - E_c(0^+)}{kT} \right) , \tag{30}$$

$$v_{n_2} = \frac{A^*T^2}{qN_{c_2}} \ . \tag{31}$$

where $v_{n_{1,2}}$ is the mean electron thermal velocity, $N_{c_{1,2}}$ is the effective density of states in the conduction band in each region, and $n_1(0^-)$ and $n_2(0^+)$ are the electron densities on either side of the heterointerface.

The net electron current density crossing at the heterointerface is

$$J_{n,i} = -qv_{n1}(1+\delta)n_1(0^-)\exp\left(-\frac{\Delta E_c}{kT} \right) + qv_{n2}(1+\delta)n_2(0^+) \tag{32}$$

The thermionic emission is taken into account through the parameter δ. When the tunneling mechanism is neglected ($\delta = 0$), this equation becomes the thermionic boundary condition.

Downloaded from SPIE Digital Library on 17 Mar 2010 to 18.51.1.125. Terms of Use: http://spiedl.org/terms

3. RESULTS AND DISCUSSIONS

We study the dependence of thermoelectromechancial loadings on barrier height and current calculated for applied potential for 10 nm and 20 nm thick $Al_xGa_{1-x}N$. The calculations are performed for a range of Al-concentration (0 to 1), temperature (0 K to 300 K), pressure (0 GPa to 10 GPa) and for 20 nm thick $Al_xGa_{1-x}N$ in 60 nm $\times$ 140 nm matrix of GaN. Figure 1 shows the band gap and conduction band edge variation under different

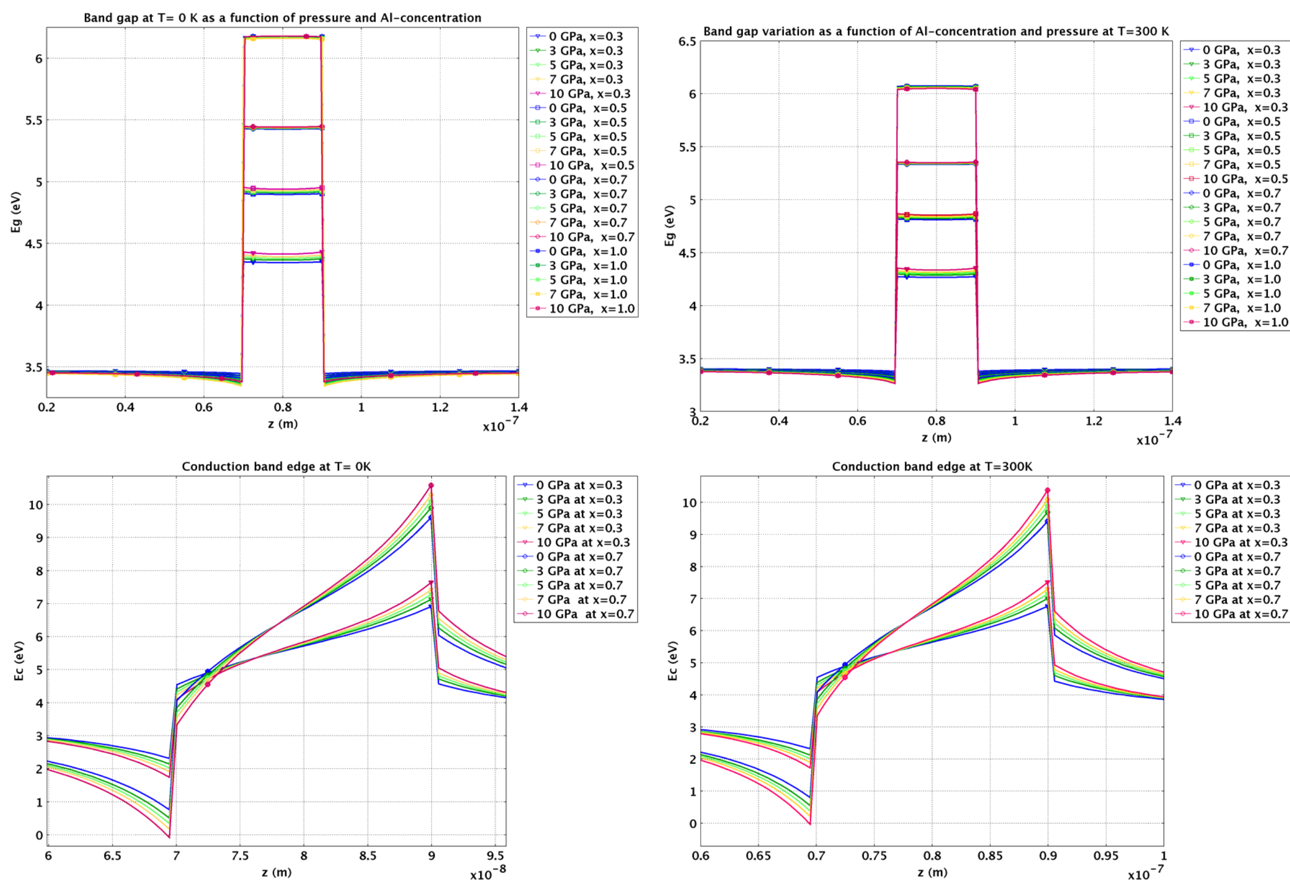

Figure 1. Effect of Al-concentration and pressure on band gap and conduction band edges of $Al_xGa_{1-x}N$/GaN heterostructure.

thermoelectromechanical loadings. The band gap energy of $Al_xGa_{1-x}N$ increases with increase in pressure and decreases with increase in temperature. E_g varies from 3.45 eV for $x = 0$ to 6.2 eV for $x = 1.0$ at T=0 K and P=0 GPa, while smaller band gapes are observed at T=300K and P=0GPa, 3.35 eV for $x = 0$ and 6.1eV for $x = 1.0$. For T=0K and 300K, the change ΔE_g is $\sim$ 0.1eV at $x = 0.3$ which further decreases to $\sim$0.0eV at $x = 1.0$. On the other hand, the conduction band edge (E_c) profiles for different x and pressure at T=0K 3 and T=300K 3 show that the change in E_c due to change in pressure, ΔE_c increases with increase in x. For T=0K and 300K, the change ΔE_c is $\sim$ 0.8eV at $x = 0.3$ which further decreases to $\sim$ 1.1eV at $x = 1.0$.

The Fermi level, η for intrinsic semiconductor can be calculated from E_g and the barrier height, ϕ_B is known from the profile of E_c for corresponding conditions. The smaller values of ΔE_g with increase in Al-concentration, may result in less sensitivity to pressure with higher Al-concentrations in $Al_xGa_{1-x}N$. On the other hand, higher values of ΔE_c with increase in Al-concentration will increase the sensitivity of the pressure sensor. However, the effect of relatively higher values of ΔE_c may overcome the effect of smaller values of ΔE_c with increase in Al-concentration and effectively may lead to increase in sensitivity of the pressure sensor at higher Al-concentrations. Figure 2 shows the pressure dependence of the current at different Al-concentrations (x = 0.3, 0.5, 0.7 and 1.0).

Downloaded from SPIE Digital Library on 17 Mar 2010 to 18.51.1.125. Terms of Use: http://spiedl.org/terms

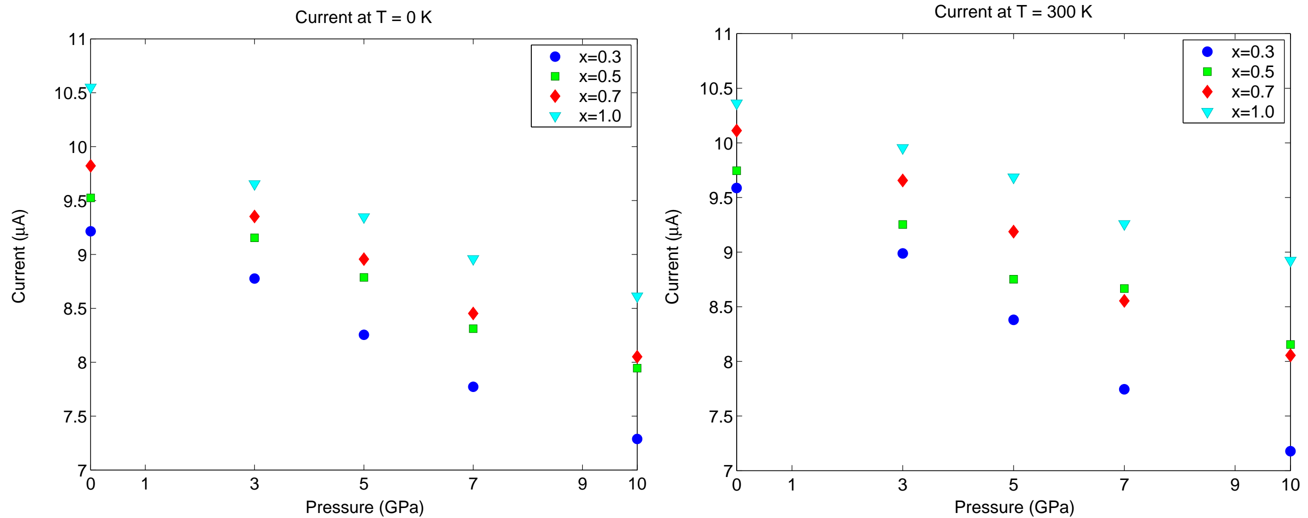

Figure 2. Calculated pressure dependence of the current as a function of Al-concentration.

The results indicate a decrease in the magnitude of the current that is nearly linear over the range of pressures from 0 to 10 GPa. This indicates that $Al_xGa_{1-x}N/GaN$ heterostructures are promising candidates for pressure sensing applications under severe environmental conditions.

4. CONCLUSIONS

In this paper, a systematic study on the effects of thermomechanical loading on $Al_xGa_{1-x}N/GaN$ heterostructures has been performed. In order to achieve this objective, a fully coupled multiphysics model incorporating balance equations for heat transfer, electrostatics and mechanical field has been developed. Using the barrier height modulation principle, we have demonstrated that $Al_xGa_{1-x}N/GaN$ heterostructures can be employed as pressure sensors under a wide range of thermal and pressure loadings. The linear trends in vertical transport current suggest the potential of these heterostructures in pressure sensor applications under severe environmental conditions.

REFERENCES

[1] J. Piprek, *Nitride Semiconductor Devices: Principles and Simulation*, Wiley-VCH, 2007.
[2] A. D. Andreev, and E. P. O Reilly, *Phys. Rev. B* **62**, 15851 (2000).
[3] A. D. Andreev, and E. P. O Reilly, *Nanotechnology* **11**, 256 (2000).
[4] B. Lassen, M. Willatzen, D. Barettin, R. V. N. Melnik, and L. C. Voon, *J. of Phys.: Conf. Series* **107**, 012008 (2008).
[5] S. R. Patil, and R. V. N. Melnik, *Nanotechnology* **20**, 125402 (2009).
[6] S. R. Patil, and R. V. N. Melnik, *Phys. Status Solidi A* **206**, 960 (2009).
[7] K. A. Son, Y. Liu, P. P. Ruden, J. Xie, N. Biyikli, Y. T. Moon, N. Onojima, and H. Markoc, *Proc. IEEE Sensors 2005* DOI: Digital Object Identifier: 10.1109/ICSENS.2005.1597935.
[8] B. S. Kang, J. Kim, F. Ren, J. W. Johnson, R. T. Therrien, P. Rajagopal, J. C. Roberts, E. L. Piner, K. J. Linthicum, S. N. G. Chu, K. Baik, B. P. Gila, C. R. Abernathy, and S. J. Pearton, *Appl. Phys. Lett.* **85**, 2962 (2004).
[9] B. S. Kang, S. Kim, J. Kim, F. Ren, J. W. Johnson, K. Baik, S. J. Pearton, B. P. Gila, C. R. Abernathy, C. C. Pan, G. T. Chen, J. I. Chyi, V. Chandrasekaran, M. Sheplak, T. Nishida, and S. N. G. Chu, *Appl. Phys. Lett.* **83**, 4845 (2003).
[10] M. Eickhoff, O. Ambacher, G. Krotz, and M. Stuzmann, *J. Appl. Phys.* **90**, 3383 (2001).

Downloaded from SPIE Digital Library on 17 Mar 2010 to 18.51.1.125. Terms of Use: http://spiedl.org/terms

[11] R. V. N. Melnik, *Appl. Math. Comput.* **107**, 27 (2000).
[12] L. C. Voon, C. Galeriu, B. Lassen, M. Willatzen, and R. V. N. Melnik, *Appl. Phys. Lett.* **87**, 041906 (2005).
[13] C. W. Nan, *Phys. Rev. B* **49**, 12619 (1994).
[14] R. V. N. Melnik, *Math. Mech. Solids* **2**, 153 (1997).
[15] R. V. N. Melnik, and K. N. Melnik, *Comm. Numer. Methods Engg.* **14**, 839 (1998).
[16] T. Nakaoka, S. Kako, and Y. Arakawa, *Physica E* **32**, 148 (2006).
[17] R. V. N. Melnik, *Comp. Phys. Commu.* **142**, 231 (2001).
[18] J. Z. Wang, P. J. Huang, Y. S. Huang, F. Firszt, S. Legowski, H. Meczynska, A. Marasek, and K. K. Tiong, *J. Phys.: Condens. Matter* **19**, 096216 (2007).
[19] S. L. Chuang, *Physics of Optoelectronic Devices*, John Wiley and Sons, 1995.
[20] K. Yang, J. R. East, and G. I. Haddad, *Solid State Electron.* **36**, 321 (1993).

Downloaded from SPIE Digital Library on 17 Mar 2010 to 18.51.1.125. Terms of Use: http://spiedl.org/terms